Journal of Medical Robotics Research, Vol. 1, No. 2 (2016) 1630001 (14 pages)
© World Scientific Publishing Company
DOI: 10.1142/S2424905X16300016

Journal of Medical Robotics Research
http://www.worldscientific.com/worldscinet/jmrr

A Compact Telemanipulated Retinal-Surgery System that Uses Commercially Available Instruments with a Quick-Change Adapter

Manikantan Nambi*,‡, Paul S. Bernstein†,§, Jake J. Abbott*,¶

*Department of Mechanical Engineering
University of Utah, Salt Lake City, UT 84112, USA

†Department of Ophthalmology and Visual Sciences
Moran Eye Center, University of Utah, Salt Lake City, UT 84123, USA

We present a telemanipulation system for retinal surgery that uses a full range of unmodified commercially available instruments. The system is compact and light enough that it could reasonably be made head-mounted to passively compensate for head movements. Two mechanisms are presented that enable the system to use commercial actuated instruments, and an instrument adapter enables quick-change of instruments during surgery. A custom stylus for a haptic interface enables intuitive and ergonomic telemanipulation of actuated instruments. Experimental results with a force-sensitive phantom eye show that telemanipulated surgery results in reduced forces on the retina compared to manual surgery, and training with the system results in improved performance.

Keywords: Eye surgery; vitreoretinal surgery; microsurgery; membrane peeling; teleoperation.

1. Introduction

Retinal microsurgery procedures are at the limits of human ability [1–5]. An error of only a few micrometers can cause the instrument to exert damaging force on the retina, causing localized loss of vision. The forces experienced during retinal surgeries are below what surgeons can feel (< 7 mN), so surgeons must rely on visual feedback only [1, 6, 7]. The surgeon must pivot the instruments about the scleral trocars (Fig. 1), limiting dexterity, and must use the instruments to manipulate the eye to provide better imaging through the surgical microscope. Patient movement due to breathing must be accounted for by the surgeon, and in addition, among patients who snore under monitored anesthesia ($\approx$16% of cases [8]), half have sudden head movements during surgery, leading to a high risk of complications.

One of the most difficult retinal surgery procedures involves the peeling of membranes on the retina. Epiretinal membrane (ERM) comprises sheets of fibrous tissue up to 61-μm-thick [9] that distort macular anatomy and disturb vision after posterior vitreous detachment or retinal tears, and the inner limiting membrane (ILM) is a naturally occurring 0.15–4-μm thick membrane [10] that can contract with age and generate macular holes. To improve vision in affected eyes, ERM and ILM are peeled by inserting delicate instruments inside the eye (Fig. 1). Membrane peeling is a delicate procedure, and complications occur frequently in the form of intraoperative hemorrhage, retinal detachment during or after surgery, infection after surgery, regrowth of ERM, and increased rate of cataract development [11]. In some cases, a second surgery is required to remove fragments of the ERM/ILM left behind. Other experimental procedures inside the eye like retinal vein cannulation involve delivering drugs to retinal veins that measure less than 100 μm in diameter, whereas physiological tremor in the human hand during retinal surgery was measured to be 100 μm [3].

Received 14 June 2015; Revised 30 August 2015; Accepted 6 October 2015; Published 13 June 2016. This paper was recommended for publication in its revised form by Editors Rajni Patel and Iulian Ioan Iordachita.
Email Addresses: ‡m.nambi@utah.edu, §paul.bernstein@hsc.utah.edu, ¶jake.abbott@utah.edu

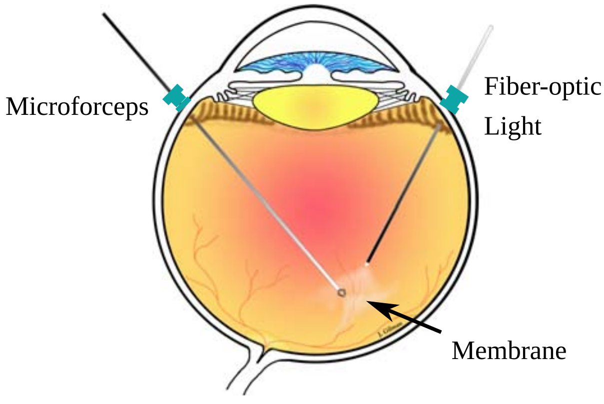

Fig. 1. Instruments inserted through trocars in the pars plana region of the sclera are used to perform delicate scraping and peeling motions to peel membranes on the retina. Image courtesy James Gilman, CRA, FOPS.

There are opportunities for significant improvement in retinal-surgery procedures in terms of safety and consistency of outcomes. As our population ages over coming years, the number of surgical procedures will likely increase relative to the number of surgeons available [12]. Robot-assisted retinal surgery will enable surgeons to improve surgical efficiency by enabling them to overcome their human limitations, and to extend their working life and capitalize on their experience even after their manual abilities have diminished.

Prior research in robot-assisted retinal surgery has resulted in the development of telemanipulated systems [13–20] and cooperative manipulators [21, 22]. Robotic systems for retinal surgery have typically been relatively large and stiff, and thus table-mounted. In related work, active hand-held instruments primarily aimed at tremor reduction, with no ability to affect the "DC" system response, have been shown to reduce RMS tremor to 10–60 μm [23–27]. Since the human hand is the source of tremor during microsurgery, telemanipulated systems, which eliminate direct contact between the surgeon and the instrument, seem particularly promising. Most prior systems leave the retina at risk in the event of sudden head movement, and rhythmic head movements would need to be actively compensated. Notable exceptions are the TU Munich [17] and Columbia/Vanderbilt systems [15], which are designed to be head-mountable. The TU Munich system [17] has been demonstrated to be head-mountable.

The specifications of retinal surgery are difficult to achieve using traditional mechatronic components (e.g. motors, gears), while maintaining a small form factor. In this paper, we present a manipulator for retinal surgery that utilizes piezoelectric stick-slip actuators, which were designed specifically for micromanipulation (this same style of actuator was used by Nasseri *et al.* [17]). Piezoelectric stick-slip actuators have a high resolution (<1 nm) and a high dynamic displacement range (cm–nm) [28]. During normal operation these actuators behave like admittance-type devices (i.e. they are stiff, they passively remain in place until actively commanded to move, and they are stationary in the event of power loss), yet they can be back-driven with a gentle force by a human hand (or any other applied force) with no damage to the device, which is significantly different behavior than a traditional admittance-type device. The manipulator presented in this paper has submicron resolution and is small and light enough to be head-mounted (although that is not demonstrated in this paper). A principal contribution of this work is an instrument adapter that enables the use of the full range of unmodified commercially available instruments, including instruments that require some form of actuation, such as microforceps and scissors, and nonactuated instruments, such as a diamond-dusted scraper (DDS), a vitrector, and a fiber-optic light. The instrument adapter also enables quick change of instruments, which is an important requirement in retinal surgery that has rarely been demonstrated in prior telemanipulated systems. We also describe a custom master input device that is inspired by an Alcon disposable microforceps, which has been designed for superior

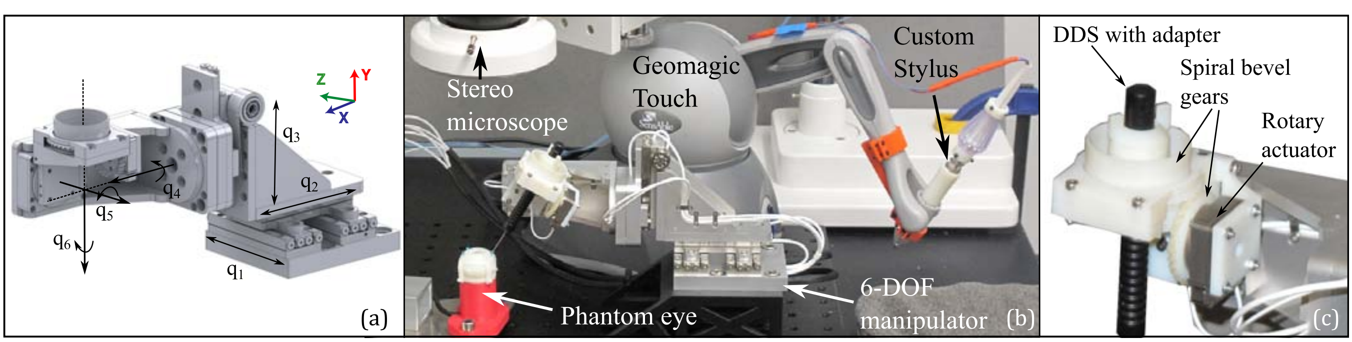

Fig. 2. (a) 6-DOF manipulator for retinal surgery. (b) Experimental setup of the retinal-surgery system. The surgeon looks in the phantom eye using a stereo microscope, and telemanipulates the end effector of the instrument with 4-DOF (3-DOF translation, and rotation of the instrument about its axis) using a Geomagic Touch (located to enable direct access to instruments) with a custom stylus that is constrained to have the same 4-DOF by locking the wrist. (c) Yaw joint of the manipulator, which is responsible for rotation of the instrument about its axis, with an adapter that enables instruments to be attached to the manipulator.

ergonomics compared to traditional pinch-grip devices. Our complete system is shown in Fig. 2. Finally, we include experimental results comparing manual membrane peeling to telemanipulated membrane peeling in a force-sensitive phantom eye. This paper is an extended treatment of an earlier work [29].

2. System Design

2.1. *6-DOF manipulator*

A six-degree-of-freedom (6-DOF) manipulator was designed using off-the-shelf piezoelectric stick-slip actuators from SmarAct GmbH (Fig. 2(a)). It comprises a 3-DOF translation stage and a 3-DOF spherical wrist, which enables the manipulator to position the instrument inside a 20-mm-diameter spherical-section bowl centered on the retina with a virtual remote center on the surface of the eye (a sphere of 25.4-mm diameter). The linear stages (q_1, q_2, and q_3) have a range of 40 mm with a closed-loop resolution of 100 nm. q_1 utilizes a parallel-rail structure, in which one rail is a stick-slip actuator and the other is a passive guide. The vertical direction (q_3) includes a constant-force spring to offset the weight of the spherical wrist. The spherical wrist comprises three rotary piezoelectric stick-slip actuators, with a closed-loop resolution of $25\,\mu^\circ$ for the roll (q_4) and pitch (q_5) actuators, and with a yaw actuator that enables open-loop rotation about the axis of the instrument (q_6) with a resolution of $3\,\mathrm{m}^\circ$. The positioning precision of the manipulator is measured with joint sensors while performing constrained motion near the retina to be $<1\,\mu$m, and the maximum velocity at the end effector is 6 mm/s. The positioning precision was verified using a VHX-5000 (Keyence Corp.) microscope. The linear actuators of the manipulator (SmarAct SLC-2460) can be backdriven by applying a force of 5 N, and the roll and pitch rotary actuators (SmarAct SR-4513, SR-2812) can be backdriven by appling torques of 15 N-cm and 6 N-cm, respectively. The maximum force that the linear actuators can apply while in motion is 4 N, and the roll and pitch actuators can apply a torque of 6 N-cm and 3 N-cm, respectively. The manipulator measures $200 \times 100 \times 70\,\mathrm{mm}^3$ and weighs 0.8 kg.

The manipulator was manufactured by SmarAct to our specifications, and we further modified the yaw joint of the manipulator such that it can use a wide range of actuated and nonactuated instruments. The modified yaw joint was manufactured using a 3D printer (Objet Eden260). The yaw joint is designed with the yaw actuator's axis orthogonal to the instrument's axis, and the rotary motion to the instrument is transmitted using spiral bevel gears. The spiral bevel gear includes a 23-mm aperture and internal threads that enable instruments to be attached to the manipulator. The aperture size was selected such that disposable instruments of a wide range of form factors can be used with the manipulator.

From our observations in the operating room, we found that during retinal surgery, on average the surgeon changes the instrument every 2 min. It is important that a robotic system for such procedures facilitates the quick change of instruments without disturbing the flow of the procedure, so we designed an adapter that enables the surgeon to change instruments frequently, and enables the use of disposable instruments that require "pinch grip" actuation such as microforceps and scissors, with this seventh DOF of actuation connected to the instrument rather than to the manipulator. Our mechanism utilizes adapters that are attached to disposable instruments before surgery. The length of each instrument is known, and the distance from the adapter base (see Fig. 3(f)) to the tip of the instrument is kept constant for each instrument. The adapters can be designed such that the shape of the adaptor conforms to the shape of a specific instrument (Figs. 3(c) and 3(f)) maintaining a constant and repeatable distance between the instrument tip and the adapter base; we have implemented a distance of 84.5 mm in our prototype, which is largely governed by the Alcon microforceps (see Fig. 3(b)). The adapter uses threads inspired by Luer fittings, and an adapter stop on the manipulator enables the instrument to be attached in the perfect position every time. Once the instruments with the adapters are attached to the manipulator, the end effector of any instrument will be at the same known location within a small tolerance (80 μm measured using images).

To characterize the instrument change time for our manipulator, we performed a simple experiment with five subjects in which the subjects changed the instrument from a DDS to a microforceps and then back to a DDS (five trials), at a comfortable speed. The time required to change an instrument was found to be $12.7\,\mathrm{s} \pm 2.5\,\mathrm{s}$ (mean $\pm$ st. dev.). We repeated this simple experiment with the same instruments for a manual surgery, and found an average change time of $8.3\,\mathrm{s} \pm 1.4\,\mathrm{s}$. With an increase in time of 5 s for every 2 min of surgery (a 4% increase), we conclude that the additional time due to tool change is fairly insignificant. By recording the joint sensor values, we confirmed that there was no motion in the joints while the instrument was being changed. Hence the instruments can be changed while the end effector is still positioned inside the eye without a risk of injuring the retina due to unintended motions during instrument change. However, additional methods will have to be used to register the exact location of the trocar on the sclera in this case.

Sterilizability is an important consideration for manipulators used in surgery. Our manipulator is small enough that it is conceivable that the entire manipulator could be gassed or autoclaved between procedures (SmarAct makes autoclavable actuators). Alternatively, all components distal to the rotary actuator shown in Fig. 2(c) (i.e. the 3D-printed components) could easily be

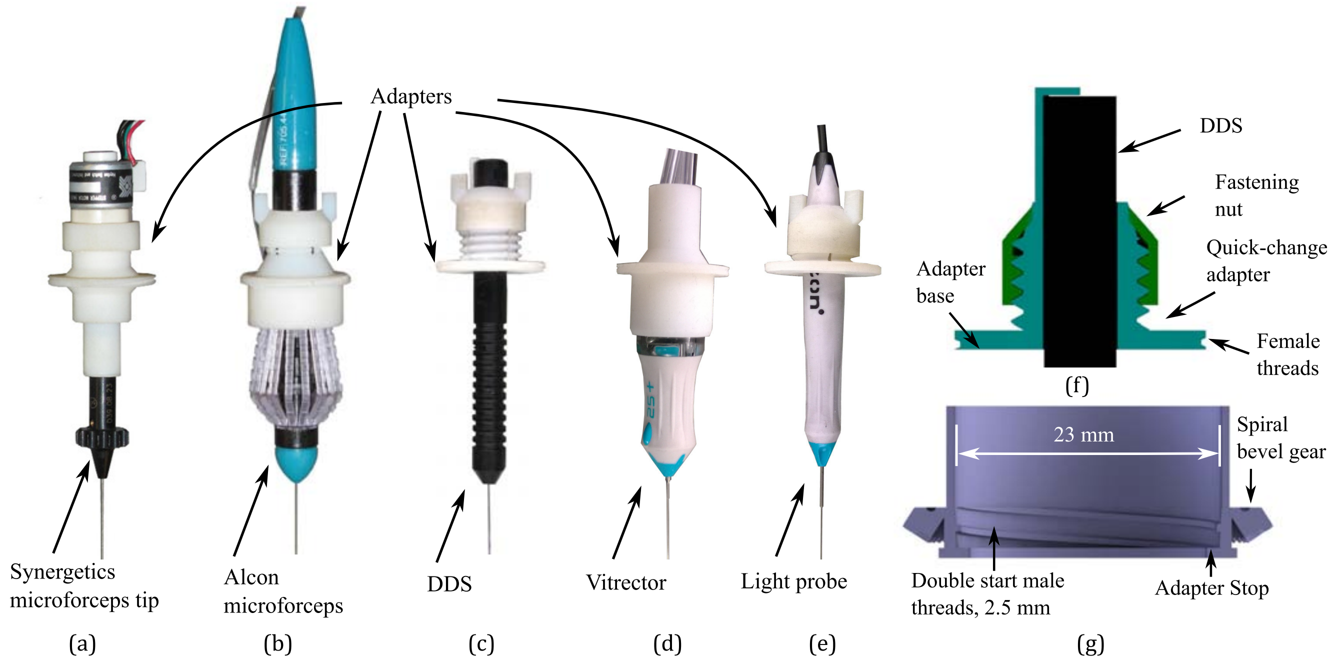

Fig. 3. (a)–(e) Disposable retinal-surgery instruments with adapters that enable quick-change mounting to the 6-DOF manipulator. (f) Section view of a quick-change adapter attached to a DDS. (g) Section view of the yaw joint to which the instruments with quick-change adapter are attached.

made disposable or removable for autoclaving. This would enable the remainder of the manipulator to be wrapped in sterile draping with a pass through for a rotary actuator's shaft, using a method inspired by that employed by Intuitive Surgical's da Vinci. Finally, we have also verified that surgical draping can be inserted between the quick-change adapter and the spiral gear on the manipulator to which the adapter is attached (Figs. 3(f) and 3(g)), and can be inserted between the linear stepper motor and the disposable microforceps tip (Fig. 4(a)) without affecting operation of the plunger, providing a potential alternate path to sterilization.

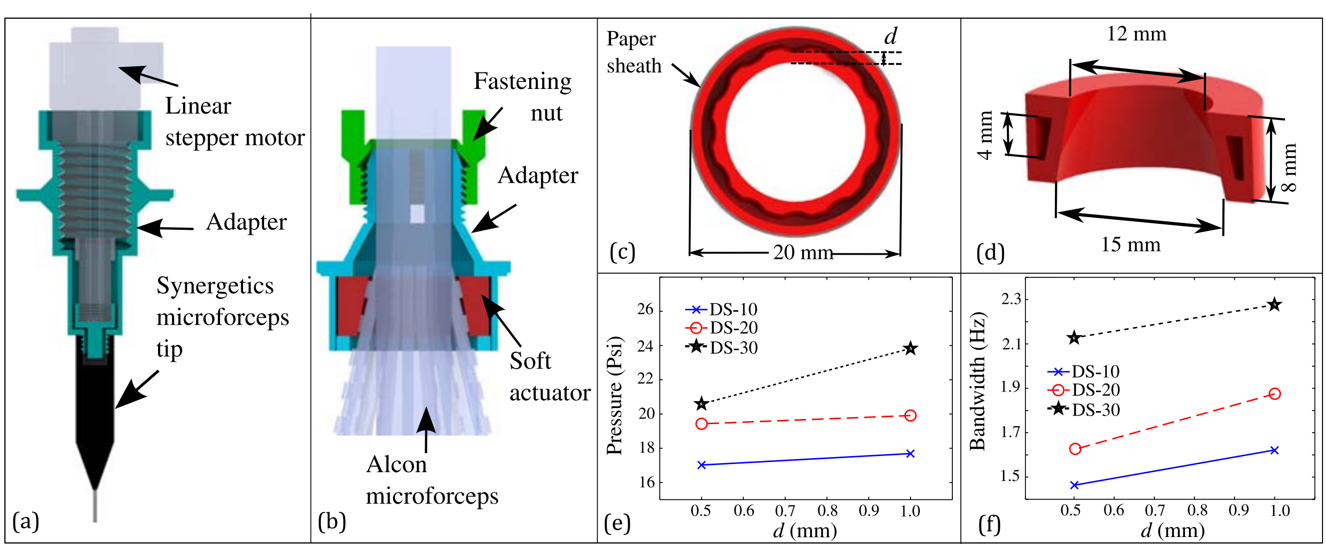

Fig. 4. (a) Section view of the Synergetics microforceps actuated by a linear stepper motor. (b) Section view of the Alcon microforceps actuated by a soft actuator. (c) Top section view of the soft actuator. The paper sheath on the outer wall and the profile of the inner wall only allow for expansion radially inward. (d) Side section view of the soft actuator. The height of the channel is inversely proportional to the maximum pressure required for actuation. (e) The maximum pressure required for complete actuation and (f) the bandwidth (for a complete open-close cycle) increases with d and the hardness of the silicone elastomer.

2.2. *Actuation mechanisms for instruments*

Two different actuation mechanisms were designed to enable the use of two different families of actuated instruments commonly used in retinal surgery: disposable instrument tips (e.g. Synergetics microforceps tip (Fig. 3(a))) that are used with reusable handles, and completely disposable instruments (e.g. Alcon microforceps (Fig. 3(b))).

2.2.1. *Actuation with stepper motor*

For actuating a disposable instrument tip, which requires pressing a plunger on the device, we used a linear stepper motor (LC15, HaydonKerk) with force capability of 5 N (2 N is required to actuate a Synergetics microforceps). The stepper motor is attached to the microforceps tip using an adapter that enables the microforceps to be mounted on the manipulator (Fig. 4(a)). The LC15 has a linear resolution of 2.5 μm, and requires 500 steps (travel of 1.25 mm) for the complete actuation (i.e., fully open to fully closed) of the microforceps. The bandwidth (measured by video analysis) for a full open-close cycle of the microforceps with the stepper motor is 2.5 Hz.

2.2.2. *Actuation with soft actuator*

The second actuation mechanism, for use with completely disposable Alcon instruments, uses a soft actuator inspired by a blood pressure cuff (Fig. 4(b)), which squeezes the ribs on a pinch-grip device when supplied with pressurized air (already available in the operating room). The soft actuator is molded from a silicone elastomer using soft-lithography techniques [30]. 3D-printed molds with inserts are used in a two-step process to fabricate the soft actuator that has a channel for pressurized air, which is then heat cured at 70°C. The inner walls of the soft actuator conform to the shape of the pinch-grip mechanism of an actuated disposable instrument (e.g. microforceps). The profile of the inner walls are designed to cause preferential expansion toward the instrument. An outer sheath made of paper is used to mitigate outward expansion of the outer wall. The soft actuators were fabricated with silicone elastomers of three different hardnesses (Dragon Skin 10, 20, and 30, Smooth-on Inc.), and two different values for the inner wall thickness d of 0.5 mm and 1 mm (see Fig. 4(c)). The soft actuator attached to an Alcon microforceps weighs 10 g, which is approximately one third that of the stepper motor-based forceps.

A PD control system comprising two ON/OFF valves (MHJ series, Festo) and a pressure sensor is implemented to regulate the pressure inside the soft actuator. The controller converts the error in pressure for the soft actuator into a PWM signal that is used to control the valves. Figure 4(e) shows that the maximum pressure required to completely close the forceps increases with the wall thickness and the elastomer hardness. A similar but counter intuitive result was observed for the bandwidth for a full open-close cycle of the forceps (Fig. 4(f)). The bandwidth increases with an increase in the wall thickness and the elastomer hardness. This can be attributed to a decrease in the deflation time for the actuators when opening the forceps, with an increase in the wall thickness and the elastomer hardness. A version of the controller with a bandwdith of 2 Hz (measured by video analysis) and a resolution of 10 discrete steps between fully open and fully closed forceps was used for experiments in Sec. 3.

2.3. *Telemanipulation system*

A Geomagic Touch (formerly known as the Phantom Omni) is used to telemanipulate the retinal manipulator. The Touch is an inexpensive haptic interface that has 6-DOF motion and sensing but only 3-DOF actuation; the position of the device's wrist can be controlled, but the orientation of the stylus cannot. We use the Touch as our master input device here for expediency; we are not advocating that it is the best device for overall performance.

A master-slave position controller is implemented in which the scaled end-effector position is mapped as a proxy point in the Touch workspace, and a virtual spring-damper is implemented between the proxy and the position of the Touch wrist. The gains were chosen to generate smooth and stable behavior. The scaled position of the Touch wrist (software-adjustable scaling, with a deadband of 200 μm on the master) is given as a position command to the end effector. A low-level position controller (Sec. 2.3.2) is implemented to servo the end effector to the desired position. A clutch (foot pedal) is used to engage/disengage the slave manipulator from the master. The remote center of motion (RCM) movement of the instrument about the trocar is handled in software, such that the user directly controls 4-DOF of end-effector movement (3-DOF Cartesian position, and rotation of the instrument about its axis). During experiments described in Sec. 3, the instrument tip is inserted into the trocar and the master pinch-grip mechanism is squeezed once to register the RCM location ($\mathbf{x}_{\mathrm{rcm}}$) in the manipulator workspace, which is fixed throughout the experiments. As there is an algorithmic singularity at the trocar, a virtual fixture is implemented for stable telemanipulation that constrains the instrument to 1-DOF instrument insertion/retraction when the end effector is near the trocar. To reduce overall experiment time in our human-subject experiments, the instruments were positioned inside the eye during trials. Orbital manipulation is not implemented here, but nothing about the design of the retinal manipulator precludes it.

In a telemanipulation experiment in which we attempted to generate the smallest possible instrument movement (five trials in each of six cardinal directions),

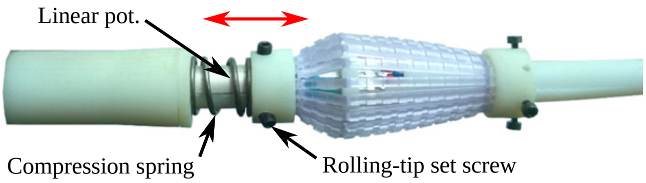

Fig. 5. Modified stylus for the Geomagic Touch. The pinch-grip mechanism from a disposable Alcon microforceps is attached to the stylus shaft, and a spring is used to recreate the stiffness of the microforceps' pinch-grip mechanism. A linear potentiometer is used to measure the squeezing of the pinch-grip mechanism.

Algorithm 1 Low-level position controller

read $\vec{x}_d, \vec{q}$
$R = \text{calculateOrientation}(\vec{x}_{rcm}, \vec{x}_d)$
$\vec{q}_d = \text{inverseKinematics}(\vec{x}_d, R)$
$\vec{dq} = \vec{q}_d - \vec{q}$
$\vec{\delta} = \text{round}(\vec{dq}/\vec{\gamma})$
$\vec{f}_{calc} = k_f \vec{\delta}/dt$
$\vec{f}_{safe} = \text{rejectFreq}(\vec{f}_{calc})$
return $\vec{\delta}, \vec{f}_{safe}$

we measured, using joint sensors, a resolution of $18.6\,\mu\text{m} \pm 9\,\mu\text{m}$ (mean $\pm$ st.dev.) with 8:1 scaling, and $2.3\,\mu\text{m} \pm 1.2\,\mu\text{m}$ with 100:1 scaling; the manipulators inherent resolution is achieved in the limit as scaling is increased.

2.3.1. *Microforceps stylus for geomagic touch*

The Geomagic Touch haptic interface is modified with a custom stylus that enables control of actuated instruments on the manipulator (Fig. 5). The stylus is built to mimic an Alcon disposable microforceps (see Fig. 3(b)), using components salvaged from its pinch-grip device. The pinch-grip mechanism is attached to a stylus, with the distal end of the mechanism allowed to move along the stylus shaft. A soft-membrane linear potentiometer (ThinPot, Spectra Symbol) is used to measure the movement of the distal end. Rolling-tip set screws at the moving distal end of the mechanism are used to reduce friction and to serve as a wiper for the potentiometer. A spring (6 N/mm) approximately recreates the stiffness of an actual microforceps. The measured position resolution of the distal end of the pinch grip mechanism is $10\,\mu\text{m}$ for a travel length of 1.25 mm.

2.3.2. *Low-level position controller*

Initial attempts at using the native closed-loop joint controllers provided by SmarAct caused undesirable vibrations at the end effector that were perceivable while telemanipulating the instrument under a microscope. As a result, we implemented a custom controller that minimizes the vibrations at the end effector to a level that they are no longer visually perceivable under a microscope.

Algorithm 1 shows the basic steps for the implemented controller that enables our manipulator to perform RCM movements about a point in its workspace ($\mathbf{x}_{\text{rcm}}$). The algorithm is called in a continuous loop by the software with a constant sampling time (dt). It takes the desired position commanded by the user ($\mathbf{x}_d$) and the current joint positions from the joint sensors ($\mathbf{q}$) as an input, and calculates the integer number of steps required along each joint ($\boldsymbol{\delta}$) with the frequency ($\mathbf{f}_{\text{safe}}$) at which the steps should be commanded in each cycle to achieve the desired position. The desired orientation vector for the end effector is calculated from the RCM point ($\mathbf{x}_{\text{rcm}}$) and the desired position ($\mathbf{x}_d$), and is converted to a desired orientation matrix (R) using Rodrigues' rotation formula. Inverse kinematics is then used to calculate the desired joint values ($\mathbf{q}_d$), and subsequently the change in joint values ($d\mathbf{q}$) required to achieve $\mathbf{x}_d$ is calculated. An empirically derived open-loop model of the step size of the joints (γ) is then used to calculate the integer number of steps ($\boldsymbol{\delta}$) required along each joint. The step size is a function of the number of steps commanded, the frequency at which the steps are commanded, and the voltage amplitude of each step. To achieve submicron precision, the voltage amplitude for each actuator is reduced by 50% when the required change in joint values (dq_i) is less than the step size of a joint i. This results in a reduced step size for the actuators.

The frequency at which each actuator should be driven ($\mathbf{f}_{\text{calc}}$) is calculated from $\boldsymbol{\delta}$ and dt. k_f is an empirically derived constant that is required for stable closed-loop operation. For our manipulator, $k_f = 0.3$. We observed that certain frequencies of operation for the rotary actuators excited the resonant frequencies of the instrument, resulting in undesirable vibrations when starting and stopping motion of the end effector. We empirically determined the undesirable frequencies by driving the rotary actuators at different frequencies and visually inspecting the vibration of the end effector. If the calculated frequency ($\mathbf{f}_{\text{calc}}$) was in the range of undesirable frequencies, it was capped to the lowest safe frequency. The range of undesirable frequencies for a DDS and a microforceps were found to be between 100 and 400 Hz. No perceivable discontinuity in the motion of the end effector was observed due to this rejection of frequencies. The SmarAct controller unit provides data from position sensors at a maximum rate of 70 Hz, and hence our controller update rate is limited to 70 Hz in this prototype. For membrane peeling during manual surgery, power analysis of the displacement of the instrument at 3 Hz has been found to be one-hundredth of the power at

DC [4]. The frequency response of our manipulator for a sinudoid of amplitude 0.5 mm at 3 Hz has an absolute amplitude gain of 0.8. As a result our manipulator is able to track all voluntary movement, and has some inherent tremor reduction since the response of the manipulator is severely attenuated at higher frequencies.

2.3.3. *Augmented controllers for retinal surgery*

During actual surgery, membranes are peeled in a circular path close to the surface of the retina, as slowly as physically possible. Peeling the membrane too fast can result in fragmentation of the membrane and can also lead to retinal tears due to excessive upward forces. Additionally, surgeons have to account for the curvature of the retina when making lateral movements close to the surface of the retina. We implemented two additional telemanipulation controllers, the *variable-speed* controller, which we hypothesized could assist in slow peeling of membranes, and the *virtual-fixture* controller, which we hypothesized could enable safer movement close to the retina. These augemented controllers are added to the *standard* telemanipulation controller already described above. In the variable-speed controller, the speed of the end effector is reduced by a somewhat-arbitrary factor of 10 if the forceps is closed by more than 10%. The closure of the forceps is taken as an intent of the user to operate on the retina, and our hypothesis is that the slower speed would improve peeling precision and reduce upward peeling forces. In the virtual-fixture controller, a virtual fixture is implemented to attenuate radial velocities toward the retina by 90% when in close proximity to the retina, whereas velocities tangent to or away from the surface remain unchanged. The virtual fixture is determined using an identification procedure by touching at least four points on the retina with the end effector, and a spherical surface that best fits the points on the retina is calculated. In clinical practice, touching the retina with instruments might not be feasible. Alternative methods that use force-sensing instruments or an optical coherance tomorgraphy (OCT) probe could be used [31, 32].

3. Experiments

3.1. *Methods*

To compare manual versus telemanipulated retinal surgery (using 8:1 scaling exclusively), we performed experiments with a phantom eye shown in Fig. 6. Trocars were inserted into the model eye as would be done in surgery. The anterior (upper portion) of the eye is made of a synthetic rubber (Phake-I, 8 mm-diameter pupil) and approximates the size, shape, and feel of the human eye. The anterior of the eye was attached to a fixture as shown in Fig. 6(a), and inside the fixture an ATI Nano17-Ti force/torque sensor (noise <1 mN) was mounted with a section of a spherical surface that acts as the posterior (retinal) surface of the eye on which surgery will be performed. This mechanical isolation between the anterior and posterior of the eye ensures that only the relatively small instrument–retina interaction forces are measured by the force sensor. The anterior portion of the model eye can rotate on the fixture allowing for minor orbital manipulation, but the posterior surface that is attached to the force sensor remains static.

The retinal surface was prepared with an artificial membrane made of paper (cut to 6-mm diameter circle, 120 μm thickness), and 10 μL of an eye lubricant gel (GenTeal) was applied to the model retina by using a pipette to achieve adhesion between the model membrane and the model retina. Paper with different strength characteristics can be used to simulate different types of membranes based on their peeling difficulty. We chose a paper membrane that, according to our surgeon author, qualitatively approximated the behavior of a real membrane. The low preparation time compared to artificial membranes previously developed in the literature [33] enabled us to keep our experiment time within reasonable limits. To measure the repeatability of our artificial membrane, we performed an experiment where the membrane was peeled at different constant velocities by the manipulator. Figure 6(e) shows the upward peeling forces (F_y) at different peeling velocities (five trials for each velocity). At velocities below 3 mm/s, the upward peeling force seems to be insensitive to the velocity.

Three vitreoretinal surgeons with varying degrees of surgical experience — 20 years (expert), two years (intermediate), six months (novice) — and a graduate student with no experience in actual surgery, performed manual and telemanipulated surgery on the phantom eye setup with an Alcon microforceps and a DDS. The graduate student and expert surgeon are both authors of this paper. All the surgeons had 2 h of practice on the telemanipulated system before data was recorded. The graduate student had been using the telemanipulation system for a year. Two experiments were performed by each subject. In Experiment 1, subjects performed manual surgery, and in Experiment 2 the surgery was performed with the telemanipulated system. Each experiment was performed with two different instruments, the DDS and the microforceps, with a single instrument being used in a given trial. With the DDS, the subjects had to scrape at the edge of the membrane for 1 min as they would during an actual surgery, applying delicate but useful forces. With the microforceps, the subjects had to completely peel a membrane off the force-sensing retina, which was visually verified in each trial. The subjects were instructed that applying minimal downward force to the retina was the primary objective, with minimizing completion time as a secondary objective. In Experiment 2, trials were performed with two

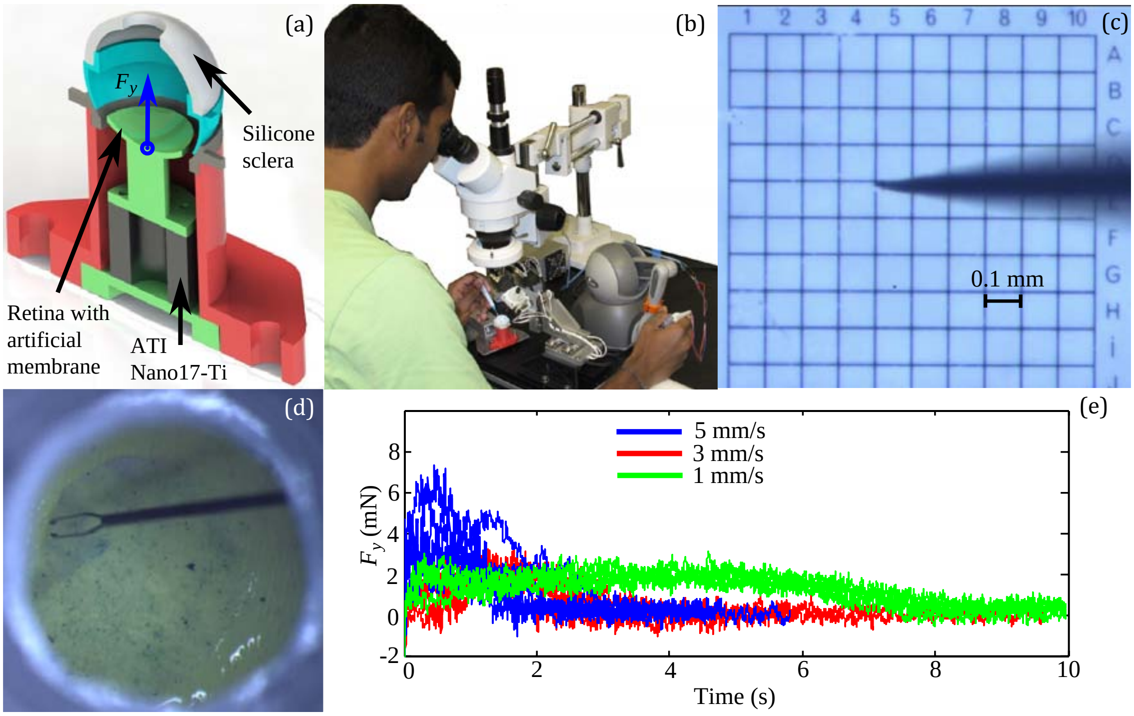

Fig. 6. (a) Phantom eye used in experiments. (b) A user performing telemanipulated surgery on the phantom eye. A fiber-optic light is manipulated manually with the left hand. (c) Snapshot from video demonstration of smooth motion across a 1 mm grid, with each subgrid measuring 100 μm, and each line having a width of approximately 8 μm. See supplementary video 1. (d) A paper membrane being peeled by an Alcon microforceps using the retinal manipulator. (e) Typical upward peeling force for the artificial membrane at different velocities.

additional controllers as described in Sec. 2.3.3 along with the standard controller. Three trials were performed in each experiment, for each instrument and controller type to obtain a total of 24 trials for a given day. Experiments were performed on two days (approximately 120 min per day) for a total of six trials per condition, and trials on a given day were randomized for instrument type and controller type (applicable only to Experiment 2). Two subjects (expert and novice) performed Experiment 1 followed by Experiment 2 on the first day, with the order reversed on the second day, and the other subjects (intermediate and graduate student) performed the experiments in a reverse order. A fresh membrane was prepared for each trial.

A third experiment was performed to measure performance in telemanipulated surgery over time, in order to measure learning effects with the robotic system without conflating factors such as switching between robotic and manual surgery. Five new subjects (four male) with no experience in performing actual surgery performed telemanipulated surgery (standard controller only) with a microforceps to peel the artificial membrane off the force-sensing retina. Subject 1 (a surgical resident) had observed membrane peeling surgery, and the other four subjects had no knowledge about the procedure. Six blocks of five trials each were performed spread across two days (three and three). The subjects were instructed that peeling the membrane while applying minimal downward force to the retina was the primary objective, with minimizing completion time as a secondary objective. After each block, the experiment conductor analyzed the data and informed the subjects that their performance could be improved by pressing even more gently on the retina, irrespective of how they had actually performed.

Although we do not purport that the experiments described in this pilot study are rigorous enough to make strong claims, we do believe that the results are informative regarding the potential of the telemanipulation system.

3.2. *Results*

To evaluate performance in our experiments, we use the maximum downward force (F_{-y}), completion time (T_c), and the maximum upward force (F_{+y}) in a given trial as independent metrics. During all microforceps experiments, the primary goal for the subjects was to minimize F_{-y}, with minimizing T_c as a secondary objective. The subjects were given no specific instruction regarding the upward peeling force F_{+y}. It should also be noted that the stiffness of the plastic used in our experiments is higher than that of an actual retina, and hence, the forces measured can only be used for comparisons within this

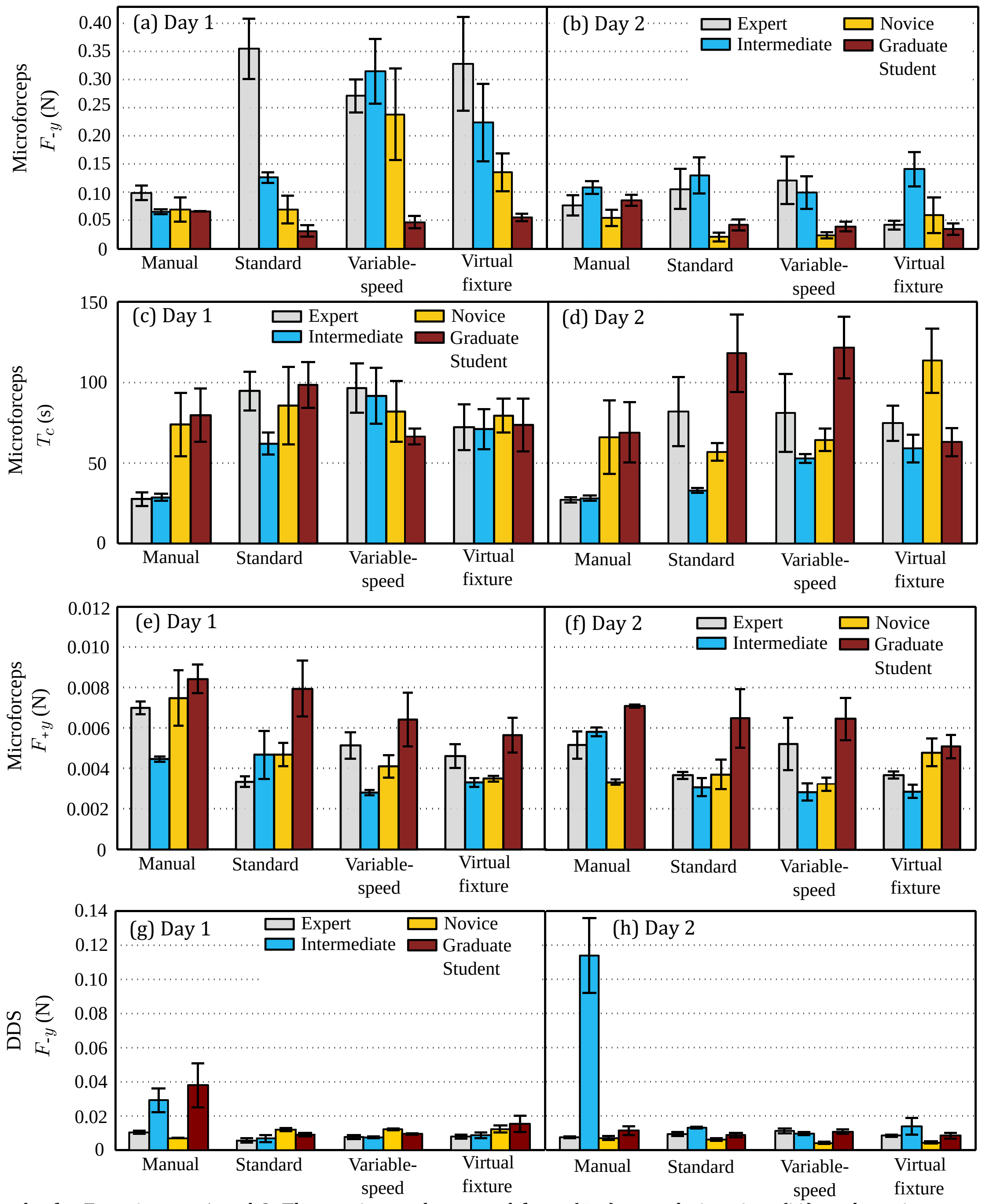

Fig. 7. Results for Experiments 1 and 2. The maximum downward force (F_{-y}), completion time (T_c), and maximum upward force (F_{+y}) for membrane peeling with a microforceps are shown in (a)–(b), (c)–(d), and (e)–(f), respectively. (g)–(h) shows maximum downward force (F_{-y}) for the scraping task with a DDS. Data is divided according to subject, day, and mode of experiment. Error bars indicate standard deviation between trials.

study, since small positioning errors can lead to relatively large rises in force.

Figure 7 shows F_{-y}, T_c, and F_{+y} for Experiments 1 and 2. For the trials performed with the microforceps, we observe that all four subjects perform approximately equivalently during manual surgery in terms of downard force F_{-y}, and that the expert and intermediate surgeons (which we will refer to as the *skilled* surgeons) perform substantially better than the other two subjects during manual surgery in terms of time T_c. We also observe there are no noticeable trends in F_{-y} (e.g. learning) from Day 1 to Day 2 for manual surgery, as we would expect, however, there is a reduction in forces for each of the telemanipulation controllers from Day 1 to Day 2 for all subjects except the graduate student suggesting that there is a learning effect from Day 1 to Day 2 for other subjects. As a result, for all subsequent analysis we lump the two days of manual data together for a given subject

Table 1. Statistically significant results ($\alpha < 0.05$) for telemanipulated membrane peeling with a microforceps for all subjects, compared against within-subject manual surgery, and against skilled-surgeon manual surgery.

		Expert			Intermediate			Novice			Grad. Student			Subjects 1–5
	Metric	S	V	F	S	V	F	S	V	F	S	V	F	S
Within-subject Manual surgery	F_{-y}	$\sim$	$\sim$	$(*)$	$\sim$	$\sim$	$\sim$	$(*)$	$\sim$	$\sim$	$*$	$*$	$*$	
	F_{+y}	$*$	$\sim$	$*$	$*$	$*$	$*$	$\sim$	$\sim$	$\sim$	$\sim$	$\sim$	$*$	
	T_c	†	†	†	$\sim$	†	†	$\sim$	$\sim$	$\sim$	$\sim$	$\sim$	$\sim$	
Skilled-surgeon Manual surgery	F_{-y}							$*$	$*$	$\sim$	$*$	$*$	$*$	$*$
	F_{+y}							$*$	$*$	$*$	$\sim$	$\sim$	$\sim$	$*$
	T_c							†	†	†	†	†	†	†

Note: S: Standard telemanipulation, V: Variable-speed controller, F: Virtual fixture controller. '$*$' indicates performance better than manual surgery, '$\sim$' indicates no significant difference was found, and '†' indicates performance worse than manual surgery. The two entries shown in parenthesis are only significant with $\alpha < 0.1$.

to increase the power of the statistics. In addition, we lump the two days of manual data for the expert and intermediate surgeons into a single *skilled* manual data set. Table 1 shows the results for independent *t*-tests comparing manual surgery to different controllers in telemanipulated surgery for each subject, and comparing telemanipulated surgery using the various controllers to both within-subject manual surgery and skilled-surgeon manual surgery (i.e. the gold standard). All statistically significant results are presented for $\alpha < 0.05$ unless specified otherwise.

We observe that the expert surgeon improves significantly from Day 1 to Day 2 with the standard and variable-speed controllers, bringing his force level down to approximately that of his manual surgery. Also, he performs better than manual surgery when using the virtual-fixture controller on Day 2 ($F(1,7) = 4.0, p = 0.08$), however, his completion time is still significantly higher than manual surgery. The upward forces during membrane peeling F_{+y} reduces significantly with the standard controller and the virtual-fixture controller as compared to manual surgery.

For the graduate student, who is an expert user with the telemanipulation system, forces are lower in telemanipulated surgery for each of the telemanipulation controllers (with Days 1 and 2 lumped together) than in manual surgery; however, his completion time may be slightly slower. We see a slight trend in reducing upward forces with the telemaniulation system as compared to manual surgery, with upward forces (F_{+y}) significantly lower with the virtual-fixture controller as compared to manual surgery. We also find that his downward forces for each of the telemanipulation controllers are significantly lower than those of the skilled surgeons' manual forces; however, his completion time is significantly longer.

Similarly, but maybe more promising, for the novice surgeon with limited surgical experience, forces are lower with the standard controller on Day 2 than in manual surgery ($F(1,7) = 3.9$, $p = 0.094$); in addition, his completion time in telemanipulated surgery is comparable to completion time in manual surgery. We also observe that the novice surgeon's downward forces with the standard controller and variable-speed controller are lower than those of the skilled surgeons' manual forces; however, his completion time is significantly longer. His upward peeling forces F_{+y} are significantly lower with all three controllers for the telemanipulated system as compared to the skilled surgeons' forces in manual surgery.

For the trials with the DDS, only F_{-y} is relevant, as the time for each trial was fixed to 1 min. From Figs. 7(g)–7(h) we observe that the intermediate surgeon performs significantly better with each of telemanipulation controllers as compared to manual surgery. We also observe the telemanipulated system helps in reducing variance in F_{-y} for the graduate student.

Figure 8 shows the experimental results for the third experiment in which five subjects performed telemanipulated membrane peeling with a microforceps with data for all the subjects combined in a single data set. We use data from the last block of experiments (Block 6) as representative of the subjects' performance after the short two-day training and compare it to the performance of the skilled surgeons in manual surgery for statistical significance. We observe a reducing trend in F_{-y}, T_c, and F_{+y} from Block 1 to Block 6. We find that with just five subjects, F_{-y} and F_{+y} in Block 6 is lower than that of manual surgery performed by the skilled surgeons with a high significance ($p < 0.001$). We observe that T_c is lower on Day 2 compared to Day 1. However, T_c in Block 6 is significantly higher than T_c for manual surgery performed by the skilled surgeons.

4. Discussion

We observed that the high positioning resolution in telemanipulated surgery (particularly in the vertical direction) often resulted in the membrane being grasped and peeled

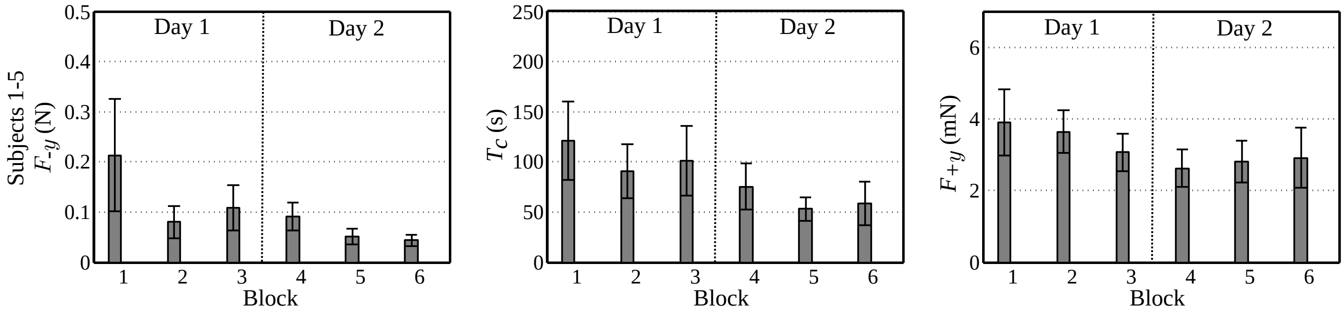

(a) (b) (c)

Fig. 8. Experimental results for telemanipulated membrane peeling with a microforceps in the phantom eye for subjects 1–5 combined. Blocks 1–3 are performed on Day 1 and Blocks 3–6 are performed on Day 2. Error bars indicate standard deviation between trials.

off in layers, with multiple grasping actions required to peel the membrane, which contributed to a higher T_c. This never manifested itself in manual surgery. It may be necessary to train users of the telemanipulator to penetrate *deep enough* into the retina to grasp the entire membrane. Additionally, we believe that the clutching required to reset the master-slave mapping also contributed to higher T_c. Also, it has been shown that positioning stability and perception of contact with the retina for skilled surgeons are significantly higher than that of surgically novice users [34]. This could explain the lower T_c for skilled surgeons as compared to novice users observed in our manual experiments.

Results from our experiments show that subjects performed better than manual membrane peeling surgery when they were trained to use the telemanipulated system over a limited period of time. In an effort to create a balanced experiment, we randomized our trials for different controllers, which we believe had a negative influence on the subjects' performance, since they were constantly having to relearn the current system's behavior. Surgeons performing robotic surgery would be trained to perform robotic surgery with the same system, and their motor skills would not have to compensate for changing system properties between trials as in our experiments. A drawback of our phantom eye setup was the lack of visual cues for forces applied on the retina. Surgeons rely on the deflection and discoloration of the retina as a measure of the force applied during membrane peeling surgery. This visual cue was lacking from our plastic retina, which could have affected our results. However, it has been shown that depth perception with visual feedback through a surgical microscope alone is similar for manual and robotic-assisted retinal surgery [35].

In terms of the achievable precision and velocity at the instrument's end effector, our manipulator compares well with other retinal-surgery manipulators (Table 2). During membrane peeling in manual surgery, instrument velocities have been measured in the range of 0.1–0.5 mm/s [7], which our manipulator is easily capable of achieving. However, we found that during bulk repositioning tasks, velocities higher than our maximum of 6 mm/s would be desirable, if the goal is to recreate instrument movements similar to manual surgery. The skilled surgeons found the velocity limit to be an annoyance. Different kinematics could be used to modify the precision-velocity trade-off. Regardless of kinematics, the quick-change adapter, disposable-instrument actuators, telemanipulation controllers, and custom stylus presented here could be utilized with almost any manipulator kinematics, including many existing systems (Table 2). Our system could also incorporate force-sensing instruments [7] for improved safety.

The augmented controllers were designed to assist in membrane peeling close to the retina. Although the surgeons saw value in the augmented controllers, they mentioned that it was harder to get used to the additional damping introduced. Subjectively, they all preferred the standard telemanipulation controller over the augmented controllers. From our experiments, we did not find any statistically significant improvement in performance by using the augmented controllers as compared to the standard telemanipulation controller. The maximum end-effector velocity was limited by the manipulator velocity and the master-slave scaling. Additionally, although our artificial membrane approximates ERM in terms of the peeling motions required, it is significantly different in terms of strength. As a result, users could peel a membrane in a single grasp-and-peel motion, which seldom happens in actual surgery. Hence the augmented controllers should be revisited and evaluated for their performance with a more realistic artificial membrane or with animal studies, or if the system is capable of achieving higher velocities, which would motivate the potential benefits of a software brake.

Due to the underactuation of our inexpensive haptic device (6-DOF with only 3-DOF actuation), we constrained our haptic device to have the same 4-DOF as the instrument's *end effector* (3-DOF translation + 1-DOF rotation) by mechanically locking the wrist angle of the

Table 2. Comparison of tele/co-manipulated retinal surgery systems. 'NA' indicates no publications or images are available.

System	Resolution/Precision	Max. velocity at the retina	Head-mountable	Quick-change/commercial actuated instruments	Surgeon input
Johns Hopkins [21]	$< 1\,\mu$m/3 μm	5 mm/s	No	Yes/No	Cooperative or Telemanipulation
Northwestern [13]	0.2 μm/$< 1\,\mu$m	NA	No	No/No	Telemanipulation
Univ. of Western Australia [14]	0.5 μm/NA	NA	No	No/No	Telemanipulation
UCLA [20]	NA/NA	NA	No	No/No	Telemanipulation
Univ. of Tokyo [16, 36]	5 μm/NA	NA	No	No/Yes	Telemanipulation
TU Eindhoven [18]	NA/10 μm	NA	No	NA/No	Telemanipulation
Univ. of Leuven [19, 22]	NA/3 μm	NA	No	NA/NA	Cooperative or Telemanipulation
Columbia/Vanderbilt [37, 31]	NA/$< 5\,\mu$m	NA	Yes	Yes/Yes	Telemanipulation
TU Munich [17]	NA/5 μm	40 mm/s	Yes	NA/NA	Telemanipulation
Univ. of Utah	0.5 μm/ $< 1\,\mu$m	6 mm/s	Yes	Yes/Yes	Telemanipulation

haptic stylus. Also, in all of our experiments, the RCM point in telemanipulated surgery was fixed, and orbital movement of the eye was not possible. As a result, the hand motions required in telemanipulated surgery with our haptic interface were fundamentally different than in manual surgery in terms of the coupling between end-effector position and instrument/stylus angle. The subjects who perform better than manual surgery with the telemanipulated system also have the least experience in real surgery. Previously developed retinal surgery telemanipulation systems have used master devices with 3-DOF translation + 1-DOF rotation [36], or with 3-DOF rotation + 1-DOF translation [18], whereas cooperative manipulators and hand-held instruments require the same hand motions as in manual surgery. It is not clear how the kinematic configuration of the master device affects the user's telemanipulation performance; this needs to be investigated further in the context of retinal surgery, potentially including the need for orbital manipulation.

Master-device kinematics aside, the control authority of the master-device actuators may also play a role in performance, particularly with the augmented controllers. The 3-DOF actuation of the Geomagic Touch used here is relatively weak, such that the highest achievable software stiffness binding the Touch's gimbal to the projected end effector is not particularly stiff compared to what could be achieved with more expensive haptic interfaces. As a result, slowing down the end-effector motion, as with the variable-speed controller, also results in a noticeable mismatch between the master and slave motions.

Experimental conditions in our study were ideal, in the sense that there was no patient eye/head movement. In actual surgery, patient head movement has to be compensated for by the surgeon. We hypothesize that all performance metrics will degrade in manual surgery when patient eye/head movement is involved, whereas a head-mounted telemanipulator will likely show comparable performance to the results obtained here. Regardless, we show that completion times for telemanipulated surgery are already comparable to manual surgery for subjects who are inexperienced in performing actual surgery.

One of the primary motivators for robot-assisted retinal surgery is to prevent the rare mistakes that can happen during manual surgery, potentially leading to surgical complication or vision loss. Sudden eye/head movement is only one potential cause of such a mistake. These rare mistakes can be difficult to capture and characterize during a structured experiment, but we see some indication of this when we consider the results of the intermediate surgeon using the DDS on Day 2, shown in Fig. 7(h); we see a large spike in downward force with no apparent reason. This is the type of mistake that can be prevented with a robotic system.

In all our experiments, subjects manually manipulated a light probe in the phantom eye with their left hand while either manually manipulating or telemanipulating the instrument with their right hand. This directly injects human hand tremor into the system, and also leads to bending of the delicate instruments when they do not work in concert, resulting in unintended motion at the end effector. To truly demonstrate the capabilities of the telemanipulated system, all manual interaction should be removed by telemanipulating both instruments.

Because of the fixed trocar point in telemanipulated surgery, the motion of the eyeball was negligible. This resulted in clear visualization of the retina which the surgeons appreciated. The skilled surgeons believe that because of the higher completion time, the telemanipulated system in its current form might not be clinically feasible for the membrane peeling procedures which they are skilled at performing. They believe that the system will be useful for experimental procedures like retinal vein cannulation and gene therapy, which are difficult for even skilled surgeons because of the high precision required.

5. Conclusion

In this paper, we have presented a telemanipulation system for retinal surgery that uses unmodified commercially available instruments. The system is compact and light enough that it could reasonably be made head-mounted in future work to passively compensate for head movements. Two actuation mechanisms were developed that enable the system to use commercially available actuated instruments, and a quick-change instrument adapter was developed that enables change of instruments during surgery. The instrument actuation mechanisms and quick-change instrument adapter could be easily adapted to work with existing retinal-surgery systems. Our experimental results with a force-sensitive phantom eye show that telemanipulated surgery shows promise in reduction of peak downward forces on the retina as compared to manual surgery for surgically novice users, and training with the system results in improved performance.

Acknowledgments

This project was funded by Intuitive Surgical Technology Research Grants and an unrestricted departmental grant to the Moran Eye Center from Research to Prevent Blindness. The authors would like to thank Alexandra Shamir for her technical assistance, Dr. Nikhil Batra and Dr. Jim Bell for their assistance with surgical equipment, Dr. Stephen Mascaro for allowing use of his lab equipment, and SmarAct GmbH for technical support. This work made use of University of Utah shared facilities of the Micron Microscopy Suite sponsored by the College of Engineering, Health Sciences Center, Office of the Vice President for Research, and the Utah Science Technology and Research (USTAR) initiative of the State of Utah.

References

1. P. K. Gupta, P. S. Jensen and E. de Juan Jr., Surgical force and tactile perception during retinal microsurgery, *Int. Conf. Medical Image Computing and Computer-Assisted Intervention*, Vol. 1679 (1999), pp. 1218–1225.
2. A. D. Jagtap and C. N. Riviere, Applied force during vitreoretinal microsurgery with handheld instruments, *Int. Conf. IEEE Engineering in Medicine and Biology Society* (2004), pp. 2771–2773.
3. S. P. N. Singh and C. N. Riviere, Physiological tremor amplitude during retinal microsurgery, *IEEE Northeast Bioengineering Conf.* (2002), pp. 171–172.
4. L. F. Hotraphinyo and C. N. Riviere, Three-dimensional accuracy assessment of eye surgeons, *IEEE Int. Conf. Engineering in Medicine and Biology Society* (2001), pp. 3458–3461.
5. C. N. Riviere, R. S. Rader and P. K. Khosla, Characteristics of hand motion of eye surgeons, *Int. Conf. IEEE. Engineering in Medicine and Biology Society* (1997), pp. 1690–1693.
6. C. N. Riviere and P. S. Jensen, A study of instrument motion in retinal microsurgery, *Int. Conf. IEEE Engineering in Medicine and Biology Society* (2000), pp. 59–60.
7. M. Balicki, A. Uneri, I. Iordachita, J. Handa, P. Gehlbach and R. Taylor, Micro-force sensing in robot assisted membrane peeling for vitreoretinal surgery, *Int. Conf. Medical Image Computing and Computer-Assisted Intervention 2010*, LNCS, Vol. 6363 (2010), pp. 303–310.
8. C. A. McCannel, E. J. Olson, M. J. Donaldson, S. J. Bakri, J. S. Pulido and D. Mueller, Snoring is associated with unexpected patient head movement during monitored anesthesia care vitreoretinal surgery, *Retina* **32**(7) (2012) 1324–1327.
9. J. R. Wilkins, C. A. Puliafito, M. R. Hee, J. S. Duker, E. Reichel, J. G. Coker, J. S. Schuman, E. A. Swanson and J. G. Fujimoto, Characterization of epiretinal membranes using optical coherence tomography, *Ophthalmology* **103**(12) (1996) 2142–2151.
10. P. B. Henrich, C. A. Monnier, M. Loparic and P. C. Cattin, Material properties of the internal limiting membrane and their significance in chromovitrectomy, *Ophthalmologica* **230**(2) (2013) 11–20.
11. G. Donati, A. D. Kapetanios and C. J. Pournaras, Complications of surgery for epiretinal membranes, *Graefe's Archive for Clinical and Experimental Ophthalmology* **236**(10) (1998) 739–746.
12. D. Harmon and J. Merritt, Demand for ophthalmic services and ophthalmologists — A resource assessment, A Study Prepared by Market Scope, LLC (2009), pp. 1–2.
13. P. S. Jensen, K. W. Grace, R. Attariwala, J. E. Colgate and M. R. Glucksberg, Toward robot-assisted vascular microsurgery in the retina, *Graefe's Arch. Clin. Exp. Ophthal.* **235**(11) (1997) 696–701.
14. D.-Y. Yu, S. Cringle and I. Constable, Robotic ocular ultra-microsurgery, *Aust. N. Z. J. Ophthalmol.* **26** (1998) S6–S8.
15. W. Wei, C. Popplewell, S. Chang, H. F. Fine and N. Simaan, Enabling technology for microvascular stenting in ophthalmic surgery, *J. Med. Dev.* **4**(1) (2010) 14503.
16. Y. Ida, N. Sugita, T. Ueta, Y. Tamaki, K. Tanimoto and M. Mitsuishi, Microsurgical robotic system for vitreoretinal surgery, *Int. J. Computer Assist. Radiol. Surg.* **7**(1) (2012) 27–34.
17. M. Nasseri, M. Eder, S. Nair, E. Dean, M. Maier, D. Zapp, C. Lohmann and A. Knoll, The introduction of a new robot for assistance in ophthalmic surgery, *Int. Conf. IEEE Engineering in Medicine and Biology Society* (2013), pp. 5682–5685.
18. H. Meenink, R. Hendrix, G. Naus, M. Beelen, H. Nijmeijer, M. Steinbuch, E. Oosterhout and M. Smet, Robot-assisted vitreoretinal surgery, in *Medical Robotics: Minimally Invasive Surgery* (2012), pp. 185–209.
19. A. Gijbels, E. Vander Poorten, P. Stalmans, H. Van Brussel and D. Reynaerts, Design of a teleoperated robotic system for retinal surgery, in *Proc. IEEE Int. Conf. Robotics and Automation*, May 2014, pp. 2357–2363.
20. E. Rahimy, J. Wilson, T. Tsao, S. Schwartz and J. Hubschman, Robot-assisted intraocular surgery: Development of the IRISS and feasibility studies in an animal model, *Eye* **27**(8) (2013) 972–978.
21. A. Uneri, M. A. Balicki, J. Handa, P. Gehlbach, R. H. Taylor and I. Iordachita, New steady-hand eye robot with micro-force sensing for vitreoretinal surgery, *IEEE Int. Conf. Biomedical Robotics and Biomechatronics* (2010), pp. 814–819.
22. A. Gijbels, E. Vander Poorten, B. Gorissen, A. Devreker, P. Stalmans and D. Reynaerts, Experimental validation of a robotic comanipulation and telemanipulation system for retinal surgery, *IEEE Int. Conf. Biomedical Robotics and Biomechatronics* (2014), pp. 144–150.
23. R. A. MacLachlan, B. C. Becker, J. Cuevas Tabarés, G. W. Podnar, L. A. Lobes and C. N. Riviere, Micron: An actively stabilized handheld tool for microsurgery, *IEEE Trans. Robot.* **28**(1) (2012) 195–212.
24. C. Song, P. L. Gehlbach and J. U. Kang, Active tremor cancellation by a "smart" handheld vitreoretinal microsurgical tool using swept source optical coherence tomography, *Opt. Express* **20**(21) (2012) 23414–23421.
25. A. Saxena and R. Patel, An active handheld device for compensation of physiological tremor using an ionic polymer metallic composite actuator, in *Proc. IEEE/RSJ Int. Conf. Intelligent Robots and Systems* (2013), pp. 4275–4280.

26. W. Latt, U.-X. Tan, C. Shee and W. Ang, A compact hand-held active physiological tremor compensation instrument, *IEEE/ASME Int. Conf. Advanced Intelligent Mechatronics* (2009), pp. 711–716.
27. C. Payne and G.-Z. Yang, Hand-held medical robots, *Ann. Biomed. Eng.* **42**(8) (2014) 1594–1605.
28. T. Higuchi and Y. Yamagata, Micro robot arm utilizing rapid deformations of peizoelectric elements, *Adv. Robot.* **6**(3) (1992) 353–360.
29. M. Nambi, P. S. Bernstein and J. J. Abbott, A Compact Retinal-surgery Telemanipulator that uses Disposable Instruments, In N. Navab *et al.* (Eds.): MICCAI 2015, Part I, LNCS 9349, pp. 258–265, Springer, 2015.
30. Y. Xia and G. M. Whitesides, Soft lithography, *Annu. Rev. Mater. Sci.* **28** (1) (1998) 153–184.
31. H. Yu, J.-H. Shen, K. M. Joos and N. Simaan, Design, calibration and preliminary testing of a robotic telemanipulator for OCT guided retinal surgery, in *Proc. IEEE Int. Conf. Robotics and Automation* (2013), pp. 225–231.
32. M. Balicki, J.-H. Han, I. Iordachita, P. Gehlbach, J. Handa, R. Taylor and J. Kang, Single fiber optical coherence tomography microsurgical instruments for computer and robot-assisted retinal surgery, *Int. Conf. Medical Image Computing and Computer-Assisted Intervention* (2009), pp. 108–115.
33. A. Gupta, B. Gonenc, M. Balicki, K. Olds, J. Handa, P. Gehlbach, R. H. Taylor and I. Iordachita, Human eye phantom for developing computer and robot-assisted epiretinal membrane peeling, *Int. Conf. IEEE Engineering in Medicine and Biology Society* (2014), pp. 6864–6867.
34. Y. Noda, Y. Ida, S. Tanaka, T. Toyama, M. F. Roggia, Y. Tamaki, N. Sugita, M. Mitsuishi and T. Ueta, Impact of robotic assistance on precision of vitreoretinal surgical procedures, *PLoS ONE* **8**(1) (2013) e54116.
35. H. Yu, J.-H. Shen, R. J. Shah, N. Simaan and K. M. Joos, Evaluation of microsurgical tasks with OCT-guided and/or robot-assisted ophthalmic forceps, *Biomed. Opt. Express* **6**(2) (2015) 457–472.
36. T. Ueta, Y. Yamaguchi, Y. Shirakawa, T. Nakano, R. Ideta, Y. Noda, A. Morita, R. Mochizuki, N. Sugita, M. Mitsuishi and Y. Tamaki, Robot-assisted vitreoretinal surgery: Development of a prototype and feasibility studies in an animal model, *Ophthalmology* **116**(8) (2009) 1538–1543.
37. H. F. Fine, W. Wei, R. E. Goldman and N. Simaan, Robot-assisted ophthalmic surgery, *Can. J. Ophthalmol.* **45**(6) (2010) 581–584.

Manikantan Nambi received his B.E. degree from the University of Mumbai, India, and his Ph.D. degree from the University of Utah, USA, in Mechanical Engineering, in 2008 and 2015, respectively. He then continued research in medical robotics as a postdoctoral researcher at the University of Utah. He is currently an engineer with Energid Technologies, USA.

Paul S. Bernstein received his B.S. degree in Chemistry in 1981, and his Ph.D. degree in Pharmacology in 1988, from Harvard University, USA. He received his M.D. degree in 1988 from the Division of Health Sciences and Technology, a joint program between Harvard Medical School and the Massachusetts Institute of Technology, USA. He did a postdoctoral fellowship in Cell Biology and a residency in Ophthalmology at the Jules Stein Eye Institute, University of California, Los Angeles, USA. In 1995, he joined the faculty of the Moran Eye Center of the University of Utah, USA, where he is now a Professor of Ophthalmology and Visual Sciences. He divides his time equally between basic-science retina research and a clinical practice devoted to medical and surgical treatment of disease of the retina and vitreous.

Jake J. Abbott received his B.S. degree from Utah State University, USA, his M.S. degree from the University of Utah, USA, and his Ph.D. degree from Johns Hopkins University, USA, all in Mechanical Engineering, in 1999, 2001, and 2005, respectively. From 2006 to 2008 he was a Postdoctoral Researcher at ETH Zurich, Switzerland. In 2008, he joined the faculty of the Department of Mechanical Engineering, University of Utah, USA, where he is now an Associate Professor.